The axial crack testing model for long distance oil - gas pipeline based on magnetic flux leakage internal inspection method

Bin Liu, Lu-yao He, Hai Zhang, Yang Cao, Henrique Fernandes

PII: S0263-2241(17)30143-4
DOI: http://dx.doi.org/10.1016/j.measurement.2017.02.051
Reference: MEASUR 4636

To appear in: *Measurement*

Received Date: 11 November 2016
Revised Date: 25 January 2017
Accepted Date: 27 February 2017

Please cite this article as: B. Liu, L-y. He, H. Zhang, Y. Cao, H. Fernandes, The axial crack testing model for long distance oil - gas pipeline based on magnetic flux leakage internal inspection method, *Measurement* (2017), doi: http://dx.doi.org/10.1016/j.measurement.2017.02.051

The axial crack testing model for long distance oil - gas pipeline based on magnetic flux leakage internal inspection method

Bin Liu[1], Lu-yao He[1], Hai Zhang[2], Yang Cao[1], Henrique Fernandes[3]

1) School of Information Science and Engineering, Shenyang University of Technology, Shenyang, 110870, China

2) Department of Electrical and Computer Engineering, computer Vision and Systems Laboratory, Laval University, 1065 av. Dela Médecine, Quebec, G1V0A6, Canada

3) Department of Mechanical Engineering, Federal University of Uberlandia, 2121 Av Joao Naves de Avila, Uberlandia, 38400-902, Brazil

Abstract: Traditional pipeline magnetic flux leakage (MFL) internal technology mainly uses axial excitation method, which could not recognize the narrow crack defects in the axial direction of the pipe. In this paper, by using a linear magnetic dipole model to study the circumferential excitation method, the detection model of axial crack in pipeline is established, and the relationship between MFL signals and the geometry characteristics of axial cracks is calculated. Finally, the detection accuracy and identification method of axial cracks is analyzed. Research results show that: non-uniform magnetic field generated by circumferential excitation can effectively detect the narrow cracks in the axial direction of the pipeline and distinguish the depth and the width characteristics of cracks. However, the background magnetic fields near the magnetic poles have great influence on the detection accuracy, and the smooth interpolation method of the cubic-spline interpolation can be used to reduce the influence effectively.

Keywords: pipeline, MFL, internal detection, axial excitation, magnetic dipole

1 Introduction

Pipeline MFL internal inspection technology is the mainstream technology to maintain the safe operation of long-distance oil - gas pipeline [1-4]. This technology belongs to the monopoly technology in the world, for it is only mastered by a few

countries, for example the pipeline MFL internal inspection device produced by American GE-PII, German ROSEN represents the advanced level in the word [5-7]. At present, axial excitation is the major method of the MFL internal inspections, which use the axial distributional magnetic field lines to detect the pit, large areas of corrosion, metal loss and circumferential cracks on the pipe wall. It plays an important role to maintain the safe operation of the long distance oil-gas pipeline. However, according to the standards of the American Society of corrosion (NACE35100), the value of traditional probability of detection (POD) is 90%, and the probability of right identification (POI) is 90%. The confidence of the pipe MFL internal inspection device, denoting to the product of the POD and the POI, is approximately 80% in the international. The confidence is not high enough mainly because the existing equipment is mainly axial excitation, which could not detect the axially oriented narrow cracks, straight welds and other defects [8-10]. For the circumferential stress in the pipe is about two times of the axial stress, axial cracks are more hazardous than circumferential cracks for oil and gas pipelines [11-13]. The defects are detected in circumferential excitation by detecting the magnetized field of surround pipe circumferential distribution, namely that axial crack defects can obviously change the distribution of circumferential magnetic field. However, the magnetic filed line distribution characteristics generated by circumferential excitation mode, influencing factors of detection signal, the recognition accuracy and recognition method of axial crack is still unclear, which makes the scientific nature and credibility of the test results lack theoretical basis [14-17].

Based on the traditional MFL internal inspection method, linear magnetic dipole model is used in this paper to simulate the MFL detection method for pipeline axial crack defect, study the distribution characteristics and crack identification methods of the MFL signals under the circumferential excitation, and analyze the influence of the crack size and the background magnetic field of the magnetic pole on the detection signal. Through a lot of experiments, this paper has verified the effectiveness and feasibility of the circumferential excitation

detection method on the axial cracks detection, which can provide basis for the improvement and practical application of traditional pipeline magnetic leakage internal inspection methods.

2 Model building

2.1 Theoretical model of crack magnetic flux leakage

When the ferromagnetic metal component reaches the magnetic saturation state, the magnetic filed line will be bended at defect position, and there will be a part of the magnetic filed line leak out of the defect surface. Using magnetic sensitive component (sensor) to detect the leakage magnetic field can judge the defect existence and characteristics [18,19]. And the surface cracks can be considered as infinite lines, using equivalent linear dipole model to simulate the distribution of the MFL field [20-22], as shown in Fig. 1.

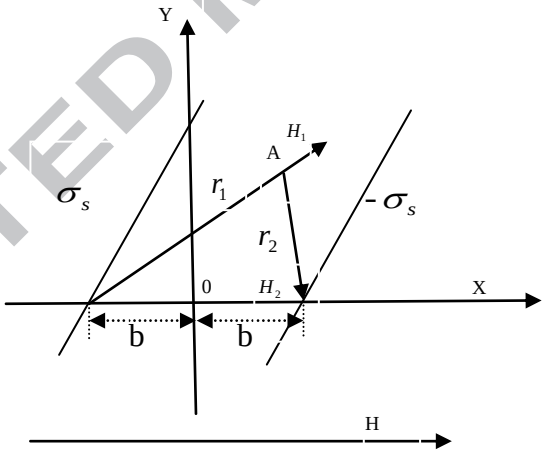

Fig.1 Linear magnetic dipole model

When applied horizontal magnetic field, line magnetic dipole consists of two infinitely long magnetic charge lines with opposing polarity, equal line magnetic charge density σ_s, and the spacing of 2b. To simplify the problem, the linear magnetic charge density σ_s is regarded as a constant (uniformly distributed magnetic charge). The field strength generated by the line element with the length of d_η at A is dH_1 and dH_2 respectively.

$$dH_1 = \frac{\sigma_s d\eta}{2\pi\mu_o r_1^2} r_1 \quad (1)$$

$$dH_2 = -\frac{\sigma_s d\eta}{2\pi\mu_o r_2^2} r_2 \quad (2)$$

Where, r_1 and r_2 is the distance from line element to A, and the component of dH_1 and dH_2 at the direction of x, y is:

$$dH_{1X} = \frac{\sigma_s (b+x)}{2\pi\mu_o[(x+b)^2 + (y+\eta)^2]} d\eta \quad (3)$$

$$dH_{2X} = \frac{\sigma_s (b+x)}{2\pi\mu_o[(x+b)^2 - (y+\eta)^2]} d\eta \quad (4)$$

$$dH_{1Y} = \frac{\sigma_s (y+\eta)}{2\pi\mu_o[(x+b)^2 + (y+\eta)^2]} d\eta \quad (5)$$

$$dH_{2Y} = \frac{\sigma_s (y+\eta)}{2\pi\mu_o[(x-b)^2 + (y+\eta)^2]} d\eta \quad (6)$$

Therefore, the total magnetic field horizontal component H_x and the vertical component H_y at the crack can be obtained by integrating to dH_x and dH_y.

$$H_x = \frac{\sigma_s (x^2 - y^2 - b^2)}{\pi\mu_o[(x+b)^2 + y^2][(x-b)^2 + y^2]} r_2 \quad (7)$$

$$H_y = \frac{2\sigma_s bxy}{\pi\mu_o[(x+b)^2 + y^2][(x-b)^2 + y^2]} r_2 \quad (8)$$

2.2 Finite element model for circumferential magnetic flux leakage (CMFL)

In the two-dimensional axisymmetric model of axial excitation, vector magnetic potential $\mathbf{A}$ only has one component, coulomb gauge $\nabla \cdot \mathbf{A} = 0$ will be automatically satisfied, which can be written as follows by using vector identities governing equation:

$$\frac{1}{\mu}\nabla^2 \mathbf{A} = -\mathbf{J} \quad (9)$$

Where, $\mathbf{J}$ is the excitation current density and μ represents the material permeability.

In the cylindrical coordinate system $(r\ \ \theta\ \ z)$, the equation can be simplified as:

$$\frac{\partial}{\partial r}\left[\frac{1}{r}\frac{\partial}{\partial r}(r\cdot A)\right]+\frac{\partial^2 A}{\partial Z^2}=-\mu J \tag{10}$$

The magnetic scalar potential and the excitation current density in the formula only have the circumferential component, which can be considered as scalar.

Magnetic structure of the internal detection system for pipeline circumferential excitation magnetic flux is symmetrical [23,24], so that the corresponding functional variational problem of Formula (10) can be described as:

$$\begin{aligned} F(A)&=2\pi\iint_s \frac{1}{2\mu}B^2\cdot r d_r d_z-2\pi\iint_s JAr d_r d_z \\ &+2\pi\int_{L_2}\frac{1}{\mu}\left[\frac{1}{2}fA_1^2-fA_2\right]r d_l \end{aligned} \tag{11}$$

Where, f is the excitation source of magnetic field, s represents the magnetic field space of the solution, L_2 is the boundary of magnetic field, $F(A)$ is the functional equation, r is the radius, A_1 and A_2 indicate the boundary value of the magnetic field space.

The magnetic filed line generated from the circumferential excitation in pipe wall is circumferential direction distributed along the pipe. Assuming that in strengthening boundary L_1 it meets that $A|_{L_1}=0$, meeting the boundaries of $\partial A/\partial Z=0$ on homogeneous natural, the Solution area partition is divided into h triangular elements, and in any triangular element e, magnetic potential A can be approximated as:

$$A=\alpha_1+\alpha_2 r+\alpha_3 z \tag{12}$$

Substituting the magnetic potential on three nodes $A_i(r_i,z_i)$、$A_j(r_j,z_j)$、$A_m(r_m,z_m)$ into Formula (12), we can get that:

$$\begin{bmatrix}\alpha_1\\ \alpha_2\\ \alpha_3\end{bmatrix}=\frac{1}{2\Delta}\begin{bmatrix}a_i & a_j & a_m\\ b_i & b_j & b_m\\ c_i & c_j & c_m\end{bmatrix} \tag{13}$$

Where,

$$\begin{aligned} a_i &= r_j z_m - r_m z_j \quad & b_i &= z_j - z_m \quad & c_i &= r_m - r_j \\ a_j &= r_m z_i - r_i z_m \quad & b_j &= z_m - z_i \quad & c_j &= r_i - r_m \\ a_m &= r_i z_j - r_j z_i \quad & b_m &= z_i - z_j \quad & c_m &= r_j - r_i \end{aligned} \tag{14}$$

Substituting α_1, α_2 and α_3 in Formula (13) into Formula (12), A^e in the element e taking node value of $A_l(l=i,j,m)$ as coefficient, the expanded form of basis functions $N_l^e(l=i,j,m)$ can be expressed as:

$$A^e = A_i N_i^e + A_j N_j^e + A_m N_m^e \tag{15}$$

$$N_l^e = \frac{1}{2\Delta}(a_l + b_l r + c_l z), l = i, j, m \tag{16}$$

By Maxwell equation [25,26], B_r^e and B_z^e in element e can be gotten:

$$B_r^e = -a_3, \quad B_z^e = \frac{A}{r} + a_2 \approx \frac{A^e}{r^e} + a_2 \tag{17}$$

So, fonctionelle $F(A)$ in Formula (11) can be written as:

$$\begin{aligned} F(A) &\approx \sum_{e=1}^{h} F^e(A) \\ &= \sum_{e=1}^{h} \left\{ 2\pi \iint_{S_e} [B^2]^e r dr dz - 2\pi \iint_{S_e} J_{0A} r dr dz \right\} \\ &\quad + 2\pi \int_{L_2} \frac{1}{\mu} \left(\frac{1}{2} f_1 A^2 - f_2 A \right) r dl \\ &= \sum_{e=1}^{h} (F_1^e + F_2^e) + F_3^e \end{aligned} \tag{18}$$

By calculating $F(A)$, coefficient matrix of boundary element in non-homogeneous natural boundary L_2 can be obtained:

$$[K]^e + [K']^e = \begin{bmatrix} K_{ii}^e & K_{ij}^e & K_{im}^e \\ K_{ji}^e & K_{jj}^e + \dfrac{\pi\varepsilon\, l_0 f_1}{2}\left(r_j + \dfrac{r_m}{3}\right) & K_{jm}^e + \dfrac{\pi\varepsilon\, l_0 f_1}{6}\left(r_j + \dfrac{r_m}{3}\right) \\ K_{mi}^e & K_{mj}^e + \dfrac{\pi\varepsilon\, l_0 f_1}{6}\left(r_j + \dfrac{r_m}{3}\right) & K_{mm}^e + \dfrac{\pi\varepsilon\, l_0 f_1}{2}\left(r_j + \dfrac{r_m}{3}\right) \end{bmatrix} \tag{19}$$

Where, l_0 is the length of each small unit in the border L_2, $[K]^e$ is the contribution of non-homogeneous natural boundary L_2 to boundary element coefficient matrix, and $[K']^e$ is the contribution of non-homogeneous natural boundary L_2 to the excitation matrix of boundary element.

Taking extreme value for $F(A)$, that is,

$$\frac{\partial F(A)}{\partial A_i} = 0 \tag{20}$$

The linear equations for the function value A_i of n nodes are:

$$\begin{bmatrix} k_{11} & k_{12} & \cdots & k_{1n} \\ k_{21} & k_{22} & \cdots & k_{2n} \\ \vdots & \vdots & \ddots & \vdots \\ k_{n1} & k_{n2} & \cdots & k_{nn} \end{bmatrix} \begin{bmatrix} A_1 \\ A_2 \\ \vdots \\ A_n \end{bmatrix} = \begin{bmatrix} P_1 \\ P_2 \\ \vdots \\ P_n \end{bmatrix} \tag{21}$$

Where, $k_{ij} = \sum_{e=1}^{h} (k_{ij}^e + k_{ij}'^e)$, $P_i = \sum_{e=1}^{h} (P_i^e + P_i'^e)$。

The value of A_i on n nodes can be obtained by solving Formula (21), and then the distribution of magnetic induction intensity B in the whole space can be obtained.

2.3 Simulation for circumferential excitation

Magnetic structure of circumferential excitation is circular symmetry, selecting 1/4 circular ring as the subject investigated, as shown in Fig. 2.

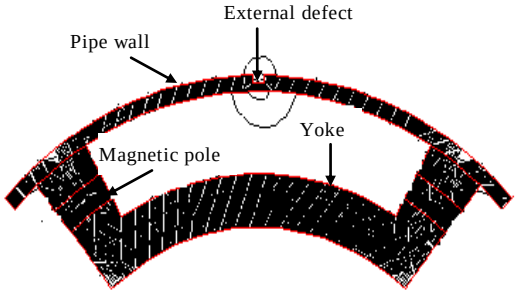

(a) Flux lines distribution of pipe with external defect

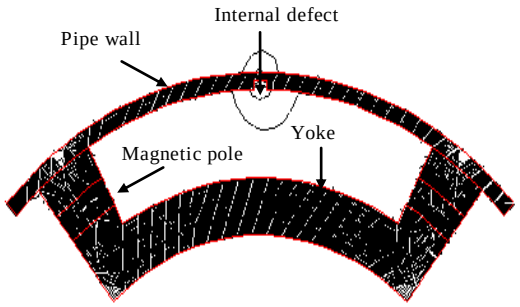

(b) Flux lines distribution of pipe with internal defect

Fig. 2 Flux lines distribution of circumferential MFL

The magnetic filed line generated from circumferential excitation method is perpendicular to the axis of the pipeline, and the axially extending crack is perpendicular to the magnetic filed line. In the presence of axial crack defects, leakage magnetic field will be generated in the inner and outer walls of the pipeline no matter internal and external defects.

The magnetic filed line generated from traditional pipeline axial excitation is evenly distributed among the pipeline. However, the magnetic filed line distribution characteristics of circumferential excitation are different from that of axial excitation. For it will generate non-uniform magnetic field in the pipe wall, as shown in Fig. 3, we can learn that the magnetic flux distribution in the pipe wall is not uniform, with the maximum magnetic field strength near the magnetic pole and minimum strength in the two pole center. When the pipe wall of the magnetic pole center reaches the magnetic saturation, and the pipe wall near magnetic pole reaches saturation, there will be flux leakage out of the pipe wall, generating a large background magnetic field, so as to affect crack detection and cover the leakage flux of crack.

3 Analysis on the influence factors of the circumferential excitation signal

3.1 The influence of background magnetic field of magnetic pole

It can be seen from Fig.3 that the relative position of cracks and pole is different and the magnetic flux leakage signal strength is also different. To study the influence of the background magnetic field near the magnetic poles on the

detection accuracy, under the same magnetization condition, simulating and calculating cracks with different distance between poles, the sample is shown in Tab. 1, among which t is the pipe wall thickness.

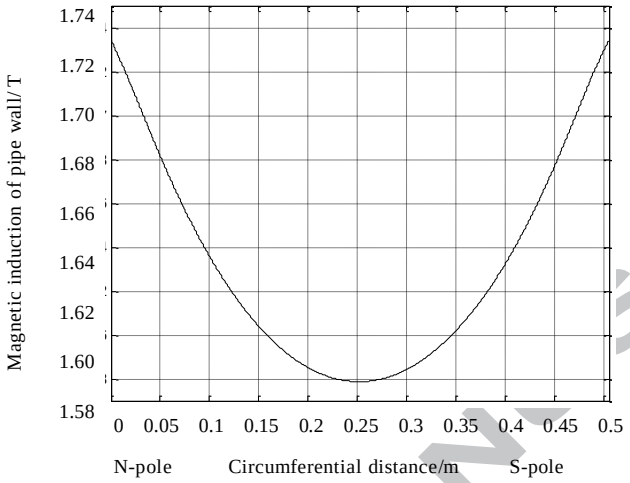

Fig.3 Magnetic induction curve at the center of the pipe wall

Under the circumferential excitation method, leakage flux distribution curve of axial crack with different characteristics in Tab. 1 is shown in Fig. 4. Because of non-uniform pipe wall magnetization and the strong magnetic field near the magnetic poles, therefore, along with the increase of the distance between the crack and the magnetic pole, the amplitude of the MFL signal is gradually reduced and the MFL signal produced by the crack defect with the distance of 30 degrees from the magnetic pole is the weakest with center symmetry. Meanwhile, the closer near the magnetic pole, the more serious influence affected by the background magnetic field of magnetic pole, MFL signal will have distortion, and radial component B_r and circumferential component B_θ will have varying degrees of distortion, being not symmetric about the defect center. Maximum absolute value of radial component near the magnetic pole is larger than that side maximum absolute value; the circumferential component signal is tilted away from the magnetic pole.

Table 1 Samples of defects in different distances from the pole

Number	distance from the pole （degree）	Width （mm）	Depth(%t)	Length （mm）
1	6	0.1	50	25

Number	distance from the pole （degree）	Width （mm）	Depth(%t)	Length （mm）
2	10	0.1	50	25
3	15	0.1	50	25
4	20	0.1	50	25
5	30	0.1	50	25

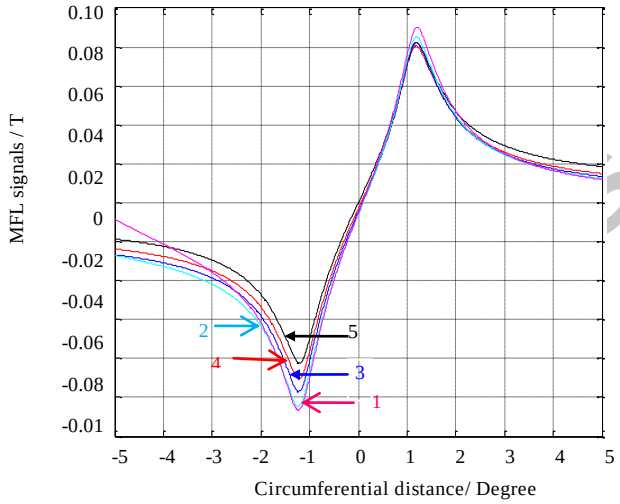

(a) Radial component

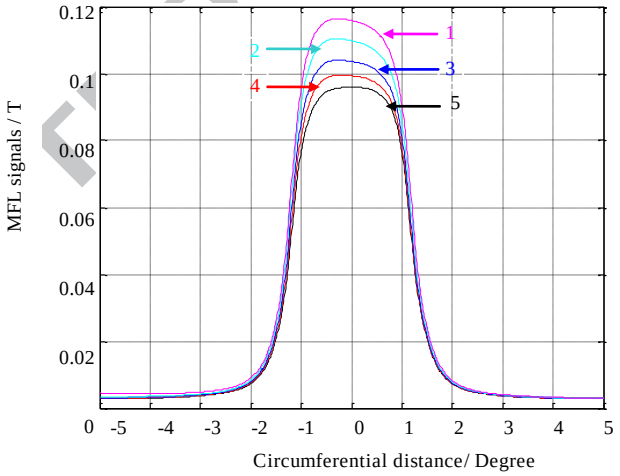

(b) Circumferential component

Fig.4 Radial MFL signals versus the defect in different distances from the pole

3.2 Influence of crack depth

Depth detection accuracy is an important indicator of the pipeline MFL internal detection technology. Under the same conditions as the width, length and magnetization, this paper studied the effect of different depth cracks on the circumferential magnetic flux leakage signals. The crack is in the center of two

magnetic poles, with width of 0.1mm, length of 25mm, and depth respectively as 1: 10%t, 2: 30%t, 3: 50%t, 4: 60%t and 5: 80%t, simulation results have been shown in Fig .5.

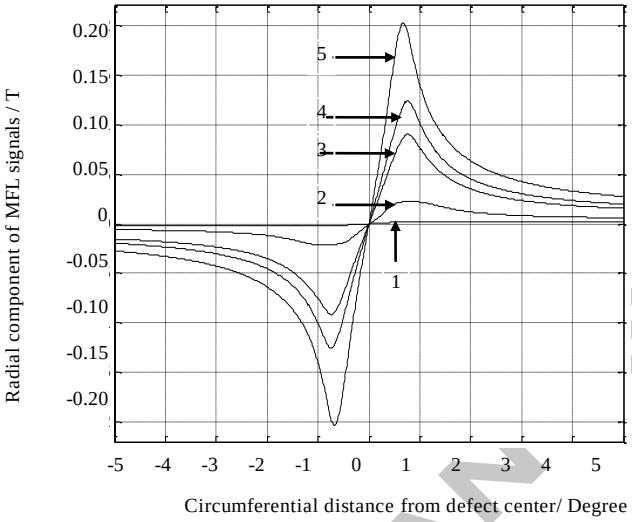

(a) Radial component

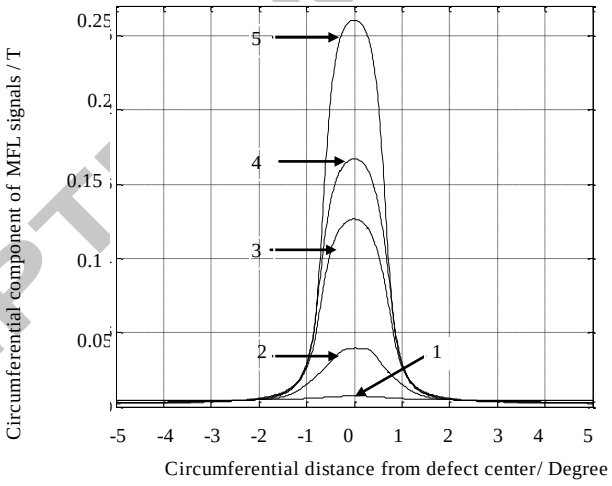

(b) Circumferential component

Fig.5 Circumferential MFL signals versus the defect depth

From Fig.5, the radial component B_r peak-to-peak value of circumferential MFL signal is increasing with the increase of the defect depth; the circumferential component B_θ peak-to-valley value is increasing with the increase of the defect depth, and the two characteristic parameters of 10%t crack is only about 1% of that of 80%t crack. From here we see that radial component B_r peak-to-peak value $B_{rp\text{-}p}$ of MFL signal and circumferential component B_θ peak-to-valley value $B_{\theta p\text{-}p}$ both

can well describe the depth of defects, which can be regarded as the characteristic quantity of evaluating defect depth.

3.3 Influence of crack width

Under the same conditions of depth, length and magnetization, the crack is in the center of two magnetic poles, with crack width respectively as 2°, 1.5°, 1°, 0.5° and 0.2°. The obtained simulation calculation of the relationship between the crack width and the radial component of the MFL signal is shown in Fig. 6, when the crack width is less 1°, the radial component B_r peak-to-peak value B_{rp-p} of MFL signal is increasing with the increase of the defect width; when the crack width is larger than 1°, B_{rp-p} is decreasing with the increase of the defect width.

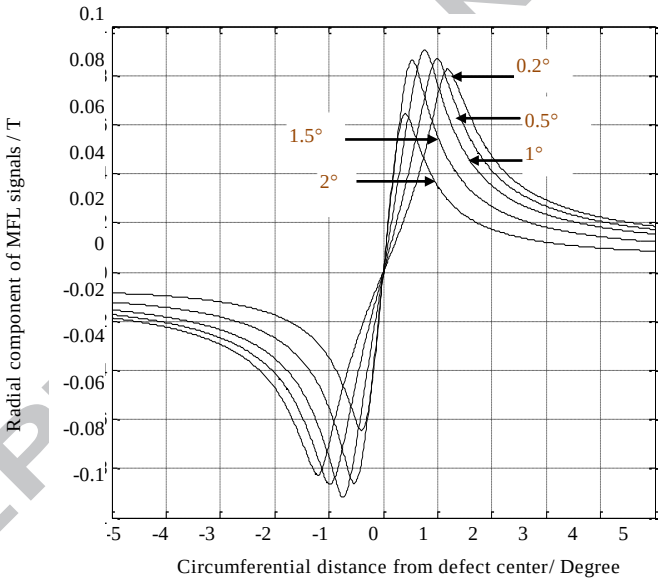

Fig.6 Radial MFL signals versus the defect width

From Fig. 6, there is no regular correspondence between the B_{rp-p} and the crack width, which can not be used as the characteristic quantity of evaluating crack width. The radial component B_r peak-to-peak spacing value S_{rp-p} is increasing with the increase of the defect width, as shown in Fig. 7, therefore, S_{rp-p} can be used to evaluate the characteristic of crack width.

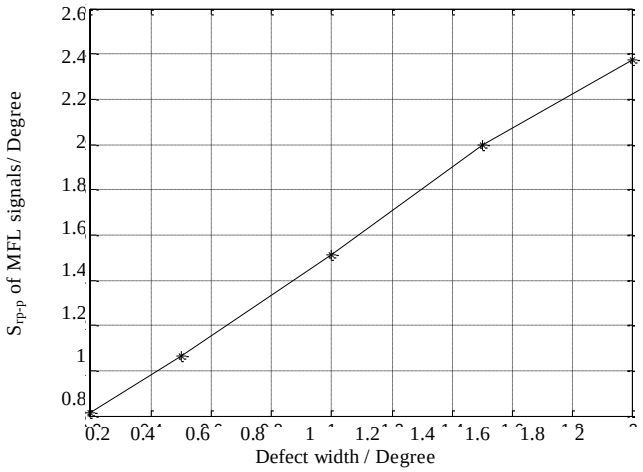

Fig. 7 Defect width versus S_{rp-p}

Circumferential component B_θ of MFL signal with different width is shown in Fig. 8. When the crack width is less than 1.5° , the crack width is narrow and the magnetic filed of the crack can be considered uniform distribution. Thus, the peak-to-valley value $B_{\theta p-p}$ of the circumference component B_θ increases as the crack width increment. This tendency is similar to the change rules of the MFL signal in axial excitation [27]; when the crack width is larger than 1.5°, the magnetic filed of the crack can be considered non-uniform distribution along the crack direction. According to the magnetic field line distribution of circumferential excitation in Fig.3, the maximum magnetic field strength is at the edge of the crack. Under the influence of end effect, $B_{\theta p-p}$ is no longer in regular changes. Therefore, there is no regularity of correspondence between $B_{\theta p-p}$ and the crack width. So $B_{\theta p-p}$ can not be used as the characteristic quantity of evaluating crack width.

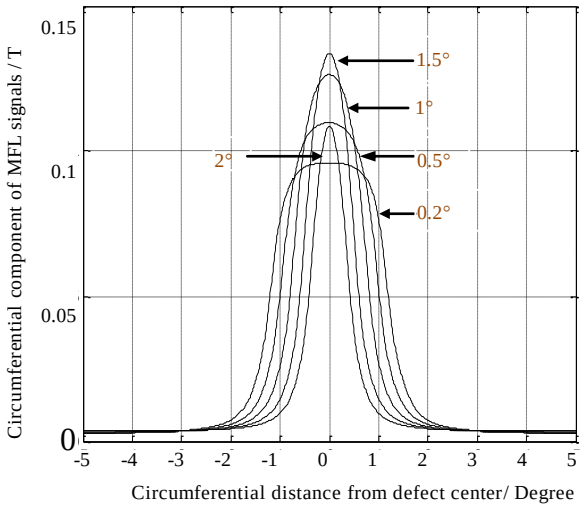

Fig.8 Circumferential MFL signals versus the defect width

However, it can be obtained in Fig.8 that the peak-to-peak spacing distance $D_{S\theta p\text{-}p}$ of the circumferential component B_θ in MFL signal is presenting a good inverse proportional linear relationship with the crack width, as shown in Fig. 9. Therefore, $D_{S\theta p\text{-}p}$ can be used as a characteristic to evaluate the crack width.

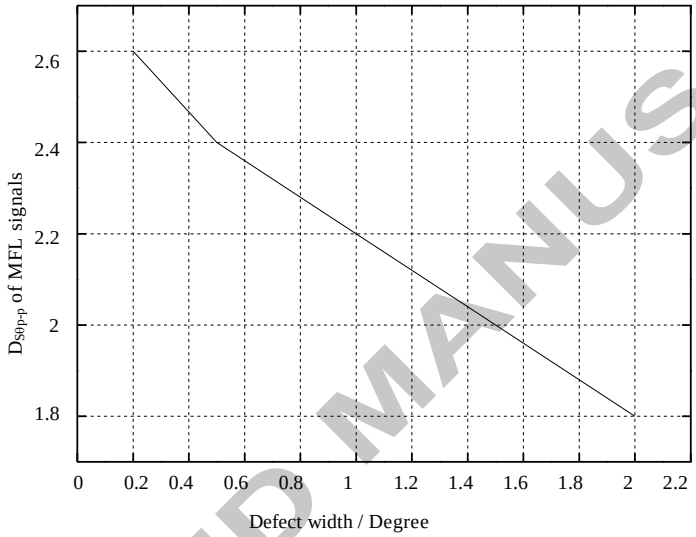

Fig. 9 Defect width versus $DS_{\theta p\text{-}p}$

3.4 Influence of crack length

Under the same conditions of crack width, depth, and magnetization, the crack is in the center of two magnetic poles, with crack width as 0.1mm, depth as 50% of pipe wall thickness, crack length respectively as 50mm, 40mm, 30mm, 20mm, 10mm and 5mm, simulation results are shown in Tab. 2, from which we can know that radial component B_r peak-to-peak value $B_{rp\text{-}p}$ and circumferential component B_θ peak-to-valley value $B_{\theta p\text{-}p}$ of MFL signal with different crack depth has unconspicuous changes; apart from the crack with length of 5mm, radial component B_r peak-to-peak spacing value $S_{rp\text{-}p}$ and circumferential component B_θ differential signal peak-to-valley spacing value $DS_{\theta p\text{-}p}$ of MFL signal basically does not change with the defect length. The calculation results show that the direction of crack length is different from that of magnetic field scanning, which

has weak effect on the leakage magnetic field generated by circumferential excitation, namely that it is difficult to determine the length of the narrow crack according to the MFL signal.

Table 2 MFL signal versus defect lengths

Number	Length/mm	$B_{rp\text{-}p}$ /T	$S_{rp\text{-}p}$ /Degree	$B_{\theta p\text{-}p}$ /T	$DS_{\theta p\text{-}p}$
1	50	0.1644	2.1625	0.12659	2.6625
2	40	0.1599	2.1625	0.12653	2.6625
3	30	0.1524	2.1625	0.12778	2.6625
4	20	0.1611	2.1625	0.12685	2.6625
5	10	0.1623	2.1625	0.12292	2.6625
6	5	0.1597	2.1725	0.12431	2.5625

4 Experiments

4.1 Experimental materials

According to the standards of the American Society of corrosion (NACE35100), with crack width larger than 0.1mm, crack length not less than the wall thickness, the crack depth detection accuracy of depth can reach 5%t. The X80 steel pipe with external diameter of 1016mm, wall thickness of 28 mm, length of 600mm is used in this paper, making axially oriented crack defect with width of 0.1mm, length of 25 mm and different depth, as shown in Tab. 3, in practical engineering application.

Table 3 Samples of artificial defects with different depth

Defects number	Length/mm	Width/mm	Depth/％wall thickness
1	25	0.1	5
2	25	0.1	10
3	25	0.1	15
4	25	0.1	20

4.2 Experimental platform

The experiment adopts the independently developed pipeline circumferential excitation detection device, as shown in Fig. 10.

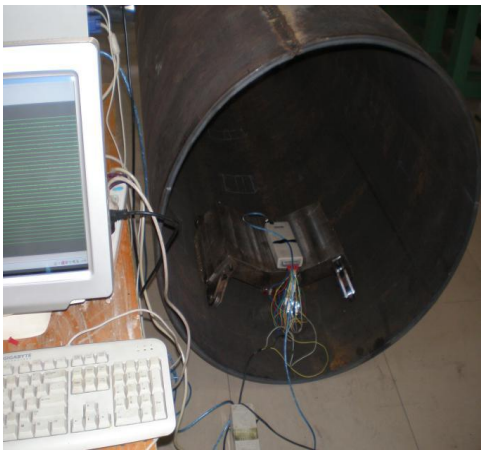

Fig.10 Experimental platform of circumferential MFL inspection

The Experimental prototype in this figure consists of magnetizer, measuring probe and wheels mounted on both ends of the magnetic device, wheels are in close contact with the pipe wall, about 1mm about air gap exists between the steel brush and pipe wall to reduce resistance, with circumferential sensor spacing of 4mm, and axial sampling frequency of 2KHz.

4.3 Experimental methods

The experimental prototype is driven by the motor through the pipe, which can be adjusted within the running speed of 0.1m/s～1.4m/s. A circumferential saturated magnetic field will be generated in the pipe wall, with experimental prototype walking in the tube. If the there is no cracks in pipe wall, the magnetic filed lines will be located within the pipe wall; If there is a crack in the inner or outer wall of the pipe, the magnetic filed line will run out of the wall generating magnetic flux leakage signal. The magnetic leakage signal is detected by the measuring probes positioned between the two magnetic poles, close to the tube wall, which is transmitted to the computer through the data acquisition card to be carried out corresponding processing and display and analyze different magnetic flux leakage signal characteristics. The experiments have been repeated five times. By comparing the peak-to-peak value $B_{rp\text{-}p}$ of the radial component B_r and the peak-to-valley value $B_{\theta p\text{-}p}$ of the circumference component with different defects, and the mean value $\bar{x}$ and the maximum deviations value δ_{max} can be obtained that is shown in Tab.1. The maximum deviations value δ_{max} within 5% proves that the experiments have a well repeatability and the experimental facilities are

stabilized.

4.4 Data processing and result analysis

4.4.1 Data processing

Under the axial excitation, the distribution of the magnetic field lines is non-uniform. It is hard to judge the characteristics of the defects from original signals because of the deep influence of the background magnetic field of the poles of MFL signals. Therefore, in practical engineering application, the smooth interpolation method of the cubic-spline interpolation can effectively reduce the influence of the non-uniform magnetic field distribution on the MFL signals.

For a given set of discrete points, the cubic-spline interpolation method is to use cubic-spline function to connect the consecutive points, and the cubic-spline interpolation curve is obtained. Because of the high smoothness (=the second order) and the approximation order (=the forth order) of the cubic-spline interpolation, the obtained curve is smooth.

Assuming that there are n+1 sampling points $a = x_0 < x_1 < \cdots < x_n = b$ in the space sampling interval [a, b], and the corresponding metrical data is $f(x_i) = y_i\ (i = 0,1,\cdots,n)$.

(1) The conditions should be satisfied by corresponding cubic-spline function is:

1) $S(x)$ is in the small interval of $[x_{i-1}, x_i](i = 1,2,\cdots,n)$;

2) $S(x)$ is second order differentiable continuous in the interval of [a, b], namely $S(x) \in C^2[a,b]$;

3) $S(x_i) = y_i\ (i = 0,1,\cdots,n)$.

Those should be recorded as: $m_i = f'(x_i)(i = 0,1,2,\cdots,n)$.

In the interval of $[x_{i-1}, x_i]$, the expression of $S(x)$ is :

$$\begin{aligned} S(x) = &\left(1 + 2\frac{x - x_{i-1}}{x_i - x_{i-1}}\right)\left(\frac{x - x_{i-1}}{x_{i-1} - x_i}\right)^2 y_{i-1} + \left(1 + 2\frac{x - x_i}{x_{i-1} - x_i}\right)\left(\frac{x - x_{i-1}}{x_i - x_{i-1}}\right)^2 y_i \\ &+ (x - x_{i-1})\left(\frac{x - x_i}{x_{i-1} - x_i}\right)^2 m_{i-1} + (x - x_i)\left(\frac{x - x_{i-1}}{x_i - x_{i-1}}\right)^2 m_i \end{aligned} \tag{22}$$

(2) Related calculated formulas

Assuming that：

$$h_{i-1} = x_i - x_{i-1} \tag{23}$$

The second derivative of the $S(x)$ is:

$$S''(x)=\left[\frac{6}{h_{i-1}^2}-\frac{12}{h_{i-1}^3}(x_i-x)\right]y_{i-1}+\left[\frac{6}{h_{i-1}^2}-\frac{12}{h_{i-1}^3}(x-x_{i-1})\right]y_i +\left[\frac{2}{h_{i-1}}-\frac{6}{h_{i-1}^2}(x_i-x)\right]m_{i-1}-\left[\frac{2}{h_{i-1}}-\frac{6}{h_{i-1}^2}(x-x_{i-1})\right]m_i \quad (24)$$

Assuming that：

$$\lambda_i=\frac{h_{i-1}}{h_{i-1}+h_i} \quad (25)$$

$$\mu_i=1-\lambda_i=\frac{h_i}{h_{i-1}+h_i} \quad (26)$$

$$d_i=3\left[\frac{\mu_i}{h_{i-1}}(y_i-y_{i-1})+\frac{\lambda_i}{h_i}(y_{i+1}-y_i)\right](i=1,2,\cdots,n-1) \quad (27)$$

Because the second derivative of $S(x)$ is continuous and differentiable, namely $S''(x_i^-)=S''(x_i^+)$, the equation set can be obtained:

$$\mu_i m_{i-1}+2m_i+\lambda_i m_{i+1}=d_i \quad (i=1,2,\cdots,n-1) \quad (28)$$

This is a n-1 liner equation set about n+1 unknown quantities m_i $(i=0,1,2,\cdots,n)$.

Assuming that the boundary condition is the natural boundary condition, the second derivative of the function $f(x)$ on the point x_0 and x_n is zero, namely that:

$$f''(x_0)=f''(x_n)=0\text{，namely that：}\ S''(x_0)=S''(x_n)=0 \quad (29)$$

The only solution m_0、m_1、⋯、m_n can be calculated by simultaneous equation sets (28) and (29).

According to the obtained sampling points and metrical data, the spline interpolation can be calculated over the interval of [a, b].

4.4.2 Result analysis

Taking a set of experiments random in Tab.4, the signal processed and analyzed by the cubic-spline interpolation is shown in Fig.11.

Table 4. Comparison of the repeatability with different depth

Experimental number	Depth/%wall thickness							
	5%t		10%t		15%t		20%t	
	$B_{rp\text{-}p}$/Sampling units	$B_{\theta p\text{-}p}$/Sampling units	$B_{rp\text{-}p}$/Sampling units	$B_{\theta p\text{-}p}$/Sampling units	$B_{rp\text{-}p}$/Sampling units	$B_{\theta p\text{-}p}$/Sampling units	$B_{rp\text{-}p}$/Sampling units	$B_{\theta p\text{-}p}$/Sampling units

1	153	54	371	272	781	337	1037	384
2	147	57	366	271	782	341	1033	387
3	150	55	370	273	780	338	1034	385
4	152	58	372	271	778	336	1032	383
5	149	53	368	275	782	340	1036	387
$\overline{X}$	150.2	55.4	369.4	272.4	781	338.4	1034.4	385.2
$\delta_{\max}$	-2.1%	4.7%	-0.9%	1.0%	0.4%	0.8%	0.3%	-0.6%

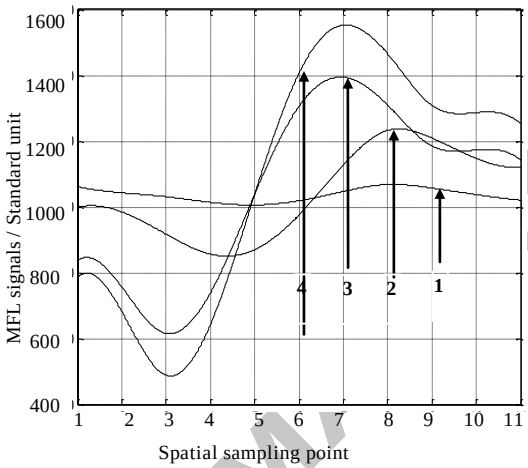

(a）Radial MFL signals

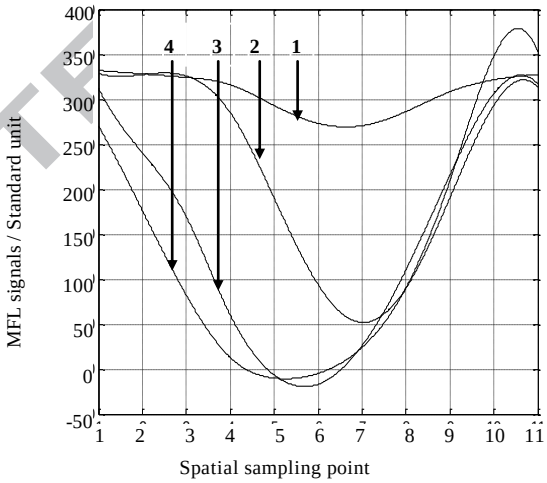

(b) Circumferential MFL signals

Fig.11 MFL signals versus the defect depth

5 Conclusions

(1)Pipeline magnetic leakage internal inspection technology uses the magnetic field formed by the circumferential excitation mode of circumferential non-uniform distributing along the pipe, and the background magnetic field near the magnetic poles is too strong, which brings a serious impact on the detection

accuracy of the crack.

(2)The crack width and depth have obvious effect on magnetic flux leakage signal generated by circumferential excitation, while the affect of crack length on magnetic flux leakage signal is less, the actual crack width and depth can be judged according to the radial component, circumferential component of magnetic flux leakage signal and differential operation.

(3)Pipeline circumferential excitation, magnetic flux leakage internal detection device can detect the axial crack defects better, but with no detectability on circumferential crack defect. So that, the combination of axial excitation and circumferential excitation can realize the pipe crack detection of full directions, which is also a development direction of long-distance oil and gas pipeline magnetic leakage internal inspection device.

(4)The combination of axial excitation and circumferential excitation on one measurement device will realize the pipeline defect detection of arbitrary direction. But in practical engineering application, the large volume of the device and the low trafficability of the pipe will cause the blockage of the inspection in pipe, resulting in the major accidents. Meanwhile, there are major differences between the changing rules of two kinds of excitation methods in MFL signal. To realize the combination of two methods needs two independent systems of data acquisition, processing and storage, which will face the problem of massive data storage. Thus, it is hard to realize the combination of axial excitation and circumferential excitation on one measurement device.

Acknowledgements

This work is funded by Project supported by the Special Funds of the National Natural Science Foundation of China (Grant No. 61141004)、the National Natural Science Foundation of China (Grant No. 60927004)and the National Key Technology Research and Development Program of the Ministry of Science and Technology of China (Grant No. 2011BAK06B01-03).

References

[1] NARA T, FUJIEDA M, GOTOH Y. Non-destructive inspection of ferromagnetic pipes based on the discrete Fourier coefficients of magnetic flux leakage[J]. Journal of Applied Physics, 2014, 115(17):17E509 - 17E509-3.

[2] LIU B, FU Y. Study on Metal Magnetic Memory Testing Mechanism[J]. Research in Nondestructive Evaluation, 2015, 1(26):1-12.

[3] YANG L J, MA F M, GAO S W. Research of On-Line Inspecting Pipeline Magnetic Flux Leakage System[J]. Chinese Journal of Scientific Instrument,2004, 25(4): 1052-1054.

[4] MANDAL K, ATHERTON D L. A study of magnetic flux-leakage signals[J]. Journal of Physics D: Applied Physics, 1998, 31(22): 3211.

[5] YANG L J, LIU B, GAO S W. Study on Magnetic Flux Leakage Testing in Weak Magnetic Field[J]. Instrument technique and sensor, 2014(1):89-92.

[6] YANG L J, CUI W T, LIU B, et al. A pipeline defect detection technique based on residual magnetism effect[J]. Oil & Gas Storage and Transportation, 2015(7):714-718.

[7] GONG W, HE R Y, ZHAO H L, et al. Cutting-edge Applications of Foreign In-line Inspection Technologies to Oil and Gas Pipeline[J]. Pipeline technology and equipment, 2013(4):24-26.

[8] YOSHIHIRO Y, YUSUKE K, TAKERU I, YOSHIHIKO U, YASUNORI T, TATSUO I. Experimental investigation of magnetic arc blow in plasma arc cutting[J]. Welding in the World, 2015, 59(1):45-51.

[9] Li X M, Ding H S, Bai S W. Research on the stress-magnetism effect of ferromagnetic materials based on three-dimensional magnetic flux leakage testing[J]. NDT&E International, 2014(62): 50-54.

[10] AMINEH R K, NIKOLOVA N K, Reilly J P, et al. Characterization of surface-breaking cracks using one tangential component of magnetic leakage field measurements[J]. IEEE Transactions on Magnetics, 2008, 44(4): 516-524.

[11] JOSHI A, UDPA L, UDPA S, et al. Adaptive wavelets for characterizing magnetic flux leakage signals from pipeline inspection[J]. IEEE transactions on magnetics, 2006, 42(10): 3168-3170.

[12] YANG L J, ZHANG G G, LIU G,et al. Design of magnetic flux leakage detection of pipeline circumferential excitation[J]. Chemical automation and instrumentation, 2010, 37(1):39-40.

[13] YANG L J, LIU F Y, GAO S W. Application of evaluation criteria for remaining strength of pipeline based on corrosion defect[J]. Journal of Shenyang University of Technology, 2014, 36(3):297-302.

[14] CHENG L，CHEN L Q，LI G L. Analysis of the Circumferential Magnetic Flux Leakage (CMFL) Signal for Oil and Gas Pipeline[J]. Pipeline Technique and Equipment, 2012(2):17-19.

[15] KANG Y H, CHEN Y T, SUN Y H. Detection Ability of MFL Inspection Under Magnetization Approaching to Saturation[J]. Nondestructive Testing, 2011(6):27-29.

[16] DENG Z Y, YANG Y, FENG B,et al. Influence of Surface Roughness on MFL Inspection of Cracks[J]. Nondestructive Testing, 2016, 38(2):40-44.

[17] PENG L S, HUANG S L, ZHAO W, et al. Defect reconstruction method for magnetic flux leakage testing[J]. Electrical measurement and instrumentation, 2015(13):1-6.

[18] YANG L J, LIN B, GAOS W, CEHN L J. First-principles caculation and experimental study of metal magnetic memory effects[J]. Chinese Journal of Physics，2013，62（8）：086201-086207

[19] HUI M K, PARK G S. A Study on the Estimation of the Shapes of Axially Oriented Cracks in CMFL Type NDT System[J]. IEEE Transactions on Magnetics, 2014, 50(2):109-112.

[20] SONGX C,YANG L, XUZ W, FEM Simulation for pipe MFL inspection under Circumferential Magnetization[J]. Chinese Journal of Mechanical Engineering, 2011, 22(22):2651-2654.

[21] MA Y L, LIN L. Research on internal and external defect identification of

drill pipe based on weak magnetic inspection[J]. INSIGHT. 2014(56):31-34.

[22] AFZAL M, UDPA S. Advanced signal processing of magnetic flux leakage data obtained from seamless gas pipeline[J]. Ndt & E International, 2002, 35(7): 449-457.

[23] STEFANITA C G. Magnetic Nondestructive Testing Techniques[J]. Magnetism .2012, 69-106.

[24] LIU B, HE L Y, ZHANG H, et al. Study on characteristics of magnetic memory testing signal on the stress concentration field[J]. IET Science, Measurement & Technology, 2017,11(1):2-8.

[25] DAVYDOV VV, VELICHKO EN. A Nutation Nuclear-Magnetic Teslameter for Measuring Weak Magnetic Fields[J]. Measurement Techniques . 2014, 57(6):684-689.

[26] G. Sposito C.Ward, P.Cawley, P.B.Nagy, C.Scruby. A review of non-destructive techniques for the detection of creep damage in power plant steels[J]. NDT & E International, 2010, 43(7): 555-567.

[27] YANG L J, GUO T H, GAO S W, et al. Feature analysis on magnetic flux leakage detection signal for special parts of oil and gas pipeline[J]. Journal of Shenyang University of Technology, 2017, 39(1): 43-47.

Highlights

1. The MFL internal inspection technology can maintain the safe operation of pipelines.

2. The axial cracks are more hazardous than circumferential cracks for pipelines.

3. The circumferential excitation method can improve the confidence of the MFL device.

4. The axial cracks can be identified by circumferential excitation method.

5. The MFL internal inspection of defects in arbitrary direction is possible to realize.